The Influence of Photorefractive Index Change on Raman Scattering Intensities in $LiNbO_3$

M. Nippus* and R. Claus

Sektion Physik der LM-Universität München, Lehrstuhl J. Brandmüller, München

Z. Naturforschung. **33a**, 924—933 (1978); received May 20, 1978

The time dependent varying shape of the laser beam within the scattering volume in Raman scattering experiments on $LiNbO_3$ influences the recorded spectra and can be studied spectroscopically by forward-, right angle-, and backward-scattering geometries. The recorded spectra allow a time resolved insight into the microscopic local changes of the refractive index. The decay constant of the scattered phonon intensity is a well defined function of the laser power. It furthermore showed to be characteristic for the individual sample. Raman spectroscopy thus seems to provide a method to determine the concentration of Fe-impurities. We have observed that ordinary photons influence the optically damaged regions of the sample whereas undamaged regions are left almost unchanged. Damped cut-in oscillations recorded when illuminating the sample alternatingly with ordinary and extraordinary laser light seem to originate from local fluctuations of an excited cloud of impurity electrons. The observation of undamped periodic break downs of the scattering intensity from polaritons and back scattered phonons is reported.

Introduction

$LiNbO_3$ exhibits a relatively large band gap in the region from 3 to about 4 eV [1]. The electronic absorption begins in the UV-region. Impurities have primarily been identified to be Fe^{++}- and Fe^{+++}-ions [2, 3, 4]. Their concentrations turned out to be at least 10 to 100 ppm. The ionization energies of these impurities are located within the band gap and thus they play the role of donors and acceptors. Depending on the wavelength of incident light Fe^{++}-ions can be excited so that electrons can reach the conduction band [5]. When using a laser in the visible to excite Fe^{++}-donors the photon density measured perpendicularly to the beam profile can be represented by a Gaussian distribution. Consequently a polarisation gradient perpendicular to the light propagation is produced along the beam path. This in turn causes an electric field removing conduction electrons from the Raman scattering volume. The electrosn may be captured by Fe^{+++}-acceptors located at approximately the same energy levels outside the beam path while producing a phonon in the lattice. The electric field in turn causes a local change of the refractive index via the electrooptic effect.

$LiNbO_3$ has an isolated absorption band near the band edge with a maximum at 21500 cm^{-1}. Its intensity varies as a function of the Fe^{++}-ion concentration. The long wavelength edge of this absorption band goes down to $\sim 14300\ cm^{-1}$ (0,7 μm) [2, 3]. The maximum has been assigned to originate from an electron transition between Fe^{++} and Nb^{5+} [2]. This means that Nb^{5+}-ions behave as acceptors in the conduction band. Since the wing of the absorption band under discussion covers almost the entire visible region, a photon-induced change of the refractive index is expected for all common (laser) wavelengths except for those in the infrared [6]. The experimental results obtained by Refs. [1 to 6] can be summarized as follows.

a) A change of birefringence is observed only for laser polarization parallel to the optic axis (z) in $LiNbO_3$.
b) The change of birefringence essentially corresponds to a change of the extraordinary refractive index. The ordinary index is left almost constant $\Delta(n^{eo} - n^{o}) \approx \Delta n^{eo}$.
c) Δn^{eo} is always negative and is of the order 10^{-3} to 10^{-5}.
d) n^{eo} decreases exponentially with time constants between 10^{-1} and 10^{3} seconds [5, 7].
e) Δn^{eo} reaches a saturation for illumination over a long time.
f) The time constants and saturation values depend on the crystal quality (Fe-concentration), temperature, and history of the sample [7].
g) The change of the refractive index can be reset by heating the sample over 170 °C, by illuminating it with UV-light, or by illumination with an unfocused expanded laser beam at the same

Reprint requests to Dr. R. Claus, Sektion Physik (Experimentalphysik) der Universität München, Schellingstr. 4/IV, D-8000 München 40

* present address: Max-Planck-Institut für Kernphysik, Projektgruppe Laserforschung, Garching.

wavelength, i.e. a homogeneous photon field without gradients.

Detailed quantitative experimental information on the band structure of $LiNbO_3$ is rare hitherto [1, 2, 8]. Studies on the electron absorption mechanism by the impurity levels in the band gap and on the optically induced electric field have been published by [7]. Various spectroscopic studies of the photorefractive effect were published recently [16]. A study of the influence on Raman scattering intensities, however, has not become known to authors.

A Simple Model for Ray Tracing

When a (focused) visible laser beam polarized in z-direction propagates through a $LiNbO_3$-sample for some time the beam becomes expanded to a cylinder cone as sketched in Figure 1a. According to Fermats' principle

$$\delta L = \delta \int_0^s n \, ds = 0 \tag{1}$$

the integral L has to remain constant for small variations of the light path between 0 and s. In order to describe our present experiments in detail the refractive index n should be considered as a function of both time and space. We eliminate the time dependence by regarding the situation after a sufficiently long illumination time only where Δn has reached a saturation $= \Delta n_\infty$. The light path then can be calculated by means of the Hamilton-Jacobi-differential equation

$$(\text{grad}\, L)^2 = n^2(x, y, z) \, . \tag{2}$$

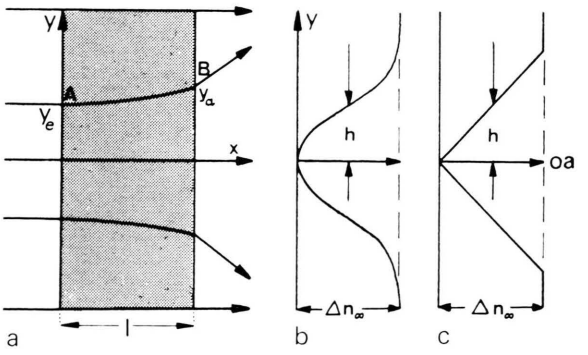

Fig. 1. a) Schematic sketch of the laser-beam-shape and path through a $LiNbO_3$-sample after a long time illumination when saturation of the extraordinary index change has been reached. b) Gaussian profile of the photon induced index change. c) Linear approximation of the index change as used in out calculations, see text.

The curvature vector $\boldsymbol{r} = (x, y, z)$ is determined by the differential equations

$$\frac{d}{ds}[n(d\boldsymbol{r}/ds)] = \nabla n \tag{3}$$

describing the light-ray trajectory in an inhomogeneous medium [9, 10]. Elementary solutions of (3) may be derived only for very simple index profiles $n(\boldsymbol{r})$. They have become of interest recently for applications in grin-rods. We reduce our present model to two dimensions as sketched in Figure 1a. The refractive index increases as a function of y from its minimum along the laser beam axis ($y = 0$). The trajectory $y(x)$ of the light beam AB can be derived by solving the light-deflection equation in the following form, see [11, 12, 13]

$$\frac{d^2y}{dx^2} = \frac{1}{n}\left[1 + \left(\frac{dy}{dx}\right)^2\right]\left[\frac{\partial n}{\partial y} - \left(\frac{dy}{dx}\right)\frac{\partial n}{\partial x}\right] . \tag{4}$$

Since $\partial n/\partial x \approx 0$ in our experiments Eq. (4) can be integrated and becomes

$$dy/dx = [(n/n_e)^2 - 1]^{1/2} \, . \tag{5}$$

Herein $n \equiv n(y)$ and $n_e \equiv n(y_e)$, according to Figure 1a. Following [11] we approximate (5) for small values of $(n/n_e)^2 - 1$

$$dy/dx = (2(n - n_e)/n_e)^{1/2} \, . \tag{6}$$

Hence it holds

$$x = \int_{y_e}^{y} [2(n - n_e)/n_e]^{-1/2} \, dy \, . \tag{7}$$

This approximation seems to be justified because $n - n_e$ normally remains $\lesssim 10^{-3}$. When introducing a Gaussian refractive index profile, see Fig. 1b, it holds $n(y) = n_0 - \Delta n_\infty \exp(-a^2y^2)$ with $n_0 \equiv n$ ($t = 0$) and $n_\infty \equiv n$ ($t \to \infty$) and the integral (7) becomes elliptic. We therefore restrict our discussion to a further simplified situation where the Gaussian distribution is replaced by a linear dependence of Δn_∞ ($\equiv n_0 - n_\infty$) on y as sketched in Figure 1c. We believe it to be advantageous to introduce all approximations in the model from the beginning rather than to use mathematical approximations later on. The linear function becomes

$$n(y) = n_\infty + \Delta n_\infty \, y/2h \, . \tag{8}$$

Equations (7) and (8) provide

$$x = \sqrt{\frac{n_e}{2}} \frac{4h}{\Delta n_\infty} \sqrt{(n_\infty - n_e) + \Delta n_\infty \, y/2h} - \sqrt{(n_\infty - n_e) + \Delta n_\infty \, y_e/2h} \, . \tag{9}$$

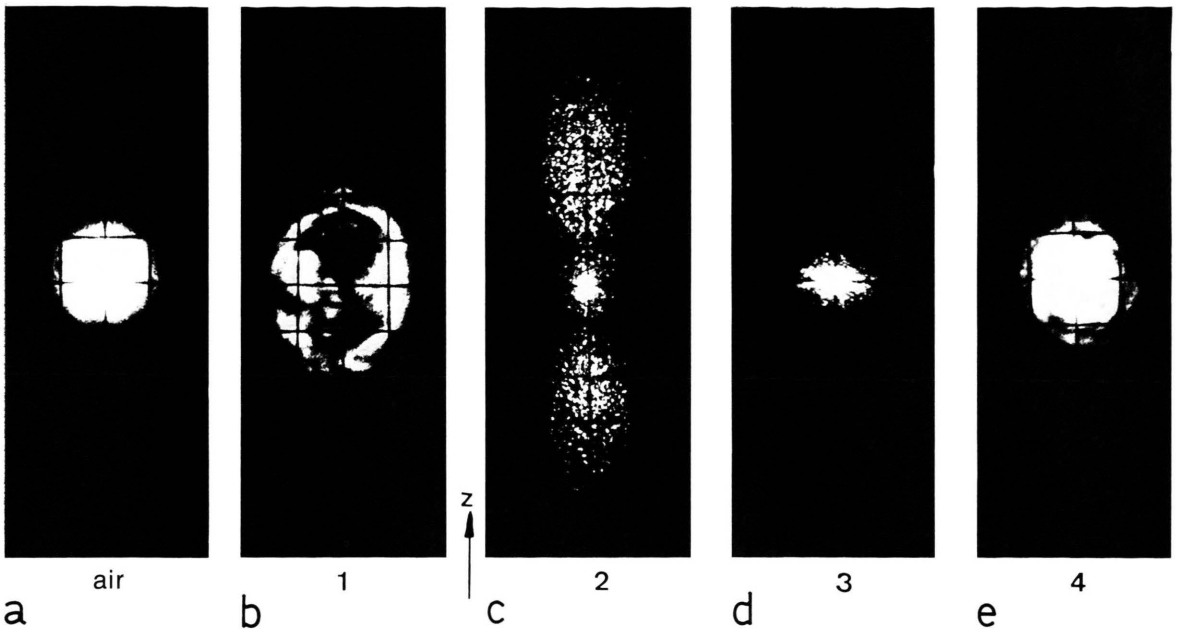

Fig. 2. a) Beam cross section in air. b) to e) Beam cross section after long time illumination: b) 10 times magnification of the image centre of c) for laser polarization $e_i \parallel z$. e) 10 times magnification of the image centre of d) for laser polarization $e_i \perp z$. An index change is recorded only for z-polarized laser light. Kr^+-laser output power $P_L = 500$ mW.

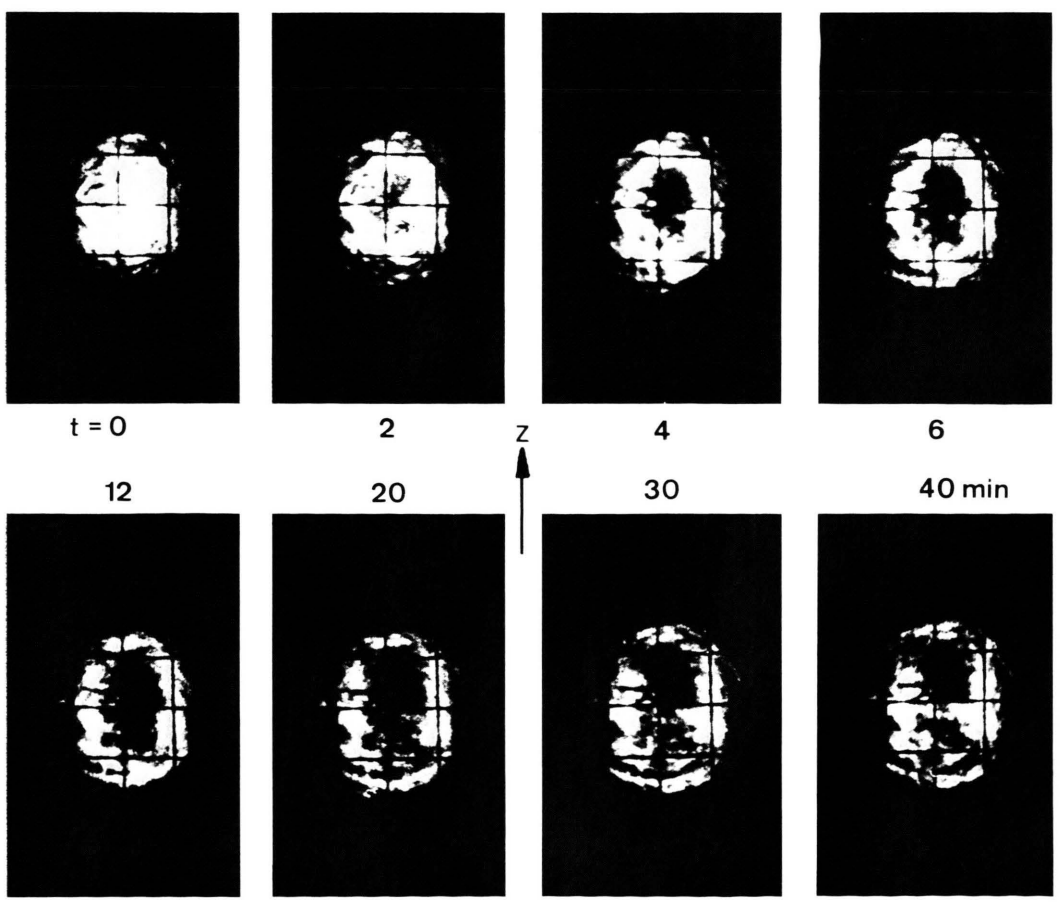

Fig. 3. Time dependence of the beam cross section. z-polarized Kr^+-laser with $P_L = 500$ mW output power.

From the photographically recorded shape of the Raman scattering volume Figs. 2 and 3, the positions of the half peak intensities can be derived. We normalize the halfwidth $2h$ by defining $h=1$. With $y_e=h=1$ and $n_e=n_\infty+\Delta n_\infty/2$ it follows from (9)

$$y=1+\frac{\Delta n_\infty x^2}{2(2n_\infty+\Delta n_\infty)}\approx 1+\frac{\Delta n_\infty x^2}{4n_\infty} \quad (10)$$

and the change of the index profile is found to be

$$\Delta n_\infty = 4n_\infty(y-1)/x^2 . \quad (11)$$

This result shall be checked by means of our experimental data below.

Experimental Results

a) The Scattering Volume Geometry

The varying shape of the scattering volume was recorded in the following way. The laser beam entered the crystal sample unfocused and the image of the emerging ray was projected on a screen at a distance of a few meters. The time dependent radial shape of the scattering volume thus could be photographed as shown in Figs. 2 and 3. All pictures were exposed and processed in such a way that the optical contrast remained unchanged. Figure 2a shows the undisturbed beam cross section. Figs. 2b and 2c are recorded after 45 min illumination of the sample. The laser beam was polarized parallel to the optic axis: $\boldsymbol{e}\parallel z$. Figure 2b is a 10 times magnification of the image centre of Figure 2c. The characteristic cylindrical form of the beam centre can be seen. Furthermore two light "clubs" in z-direction have developed. Figures 2d and 2e, on the contrary, were recorded with the laser polarization $\boldsymbol{e}\perp z$. No essential change of the beam cross section is observed. In this case Fig. 2e is a 10 times magnification of the image centre of Figure 2d. The laser output power was $P_L=500$ mW. All pictures of Fig. 2 show the situation after a long time illumination (~ 45 min) where saturation of the extraordinary index change has been reached. A remarkable index change takes place only for z-polarized laser light. The time dependent shape of the beam is shown in more detail by the pictures in Figure 3. The Raman scattering volume developes to a cylinder with weak laser intensity in the centre and maximum intensity at the positions of the half width of the original beam intensity profile. The outer and inner radii, $R(t)$ and $r(t)$, of the rings shown in Fig. 3 could be determined with a standard deviation of 6% and 15%, respectively. The radii as well as the simultaneously recorded Raman scattering intensity $I(t)$ of phonons in $LiNbO_3$ could be described by exponential time dependences. The diagrams reproduced in Fig. 4 show this. The power-area ratio of the laser changes with varying beam cross section. When assuming a cylindrical symmetry within the active scattering volume simple geometrical arguments show that the Raman intensity of phonons recorded by right angle scattering can be described in the following way

$$I=\text{const}/R^2 . \quad (12)$$

The assumption of an approximately cylindrical beam within the scattering volume is justified because the recorded divergence of the light cone actually was less than 0.5 m rad. In order to describe the time dependence of the scattering intensity quantitatively we compare $I(t)$ with its initial value $I(0)\equiv I_0$. According to (12) follows

$$I(t)/I_0=R_0^2/R^2(t) . \quad (13)$$

When furthermore introducing the stationary values R_∞, r_∞, and I_∞ recorded after long time

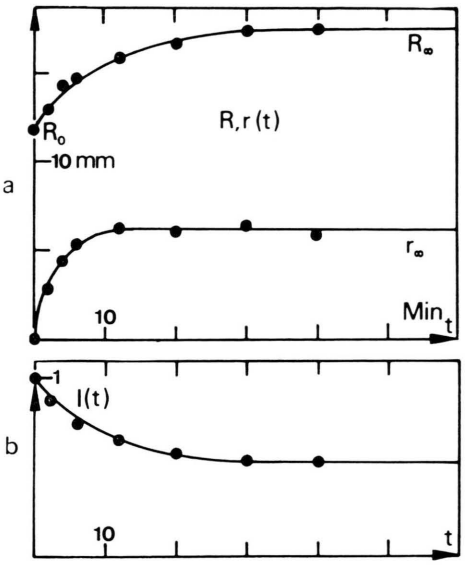

Fig. 4. Diagram showing the time dependence of the outer and inner radii $R(t)$ and $r(t)$ of the cylindrical laser beam, and phonon scattering intensities $I(t)$ in $LiNbO_3$ at relatively low laser power, see Fig. 6 and its discussion for comparison.

illumination ($t \to \infty$) the time dependences of the three quantities R, r and I are described mathematically by the following equations in a satisfactory way

$$R(t) = R_\infty + (R_0 - R_\infty)\, e^{-\alpha t}\,, \tag{14}$$

$$r(t) = r_\infty (1 - e^{-\beta t})\,, \tag{15}$$

$$I(t) = I_\infty + (I_0 - I_\infty)\, e^{-\gamma t}\,. \tag{16}$$

The numerical values of α, β, and γ obviously must be different for different samples depending on the concentration of Fe-impurities. A typical result showing the order of magnitude found in our experiments was

$$R/R_0 = 0.5\,(3 - \exp\{-0.094\, t\})\,, \tag{17}$$

$$r/R_0 = 0.5\,(1 - \exp\{-0.29\, t\})\,, \tag{18}$$

$$I/I_0 = 0.5\,(1 + \exp\{-0.094\, t\})\,. \tag{19}$$

It is worth noticing that $I(t)$ decreases with almost the same time constant as $R(t)$: $\alpha \approx \gamma = 0.094$. $r(t)$, on the other hand approaches the stationary value r_∞ much more quickly: $\beta = 0.29$. Its influence on the Raman scattering intensities thus is active over a relatively short time only in the beginning.

The time constants were found to increase with the laser power density. The time dependent Raman scattering intensities are determined essentially by the altering shape of the scattering volume. This implies, on the other hand, that the experimentally recorded function $I(t)$ also can be used to determine the time constants α and β in Eqs. (14) and (15). We checked 20 different functions $I(t)$ for varying laser output power. γ is derived most conveniently from

$$\mathrm{d}I/\mathrm{d}t = \tfrac{1}{2}\,[-\exp(-\gamma t)]\,\gamma\, I_0\,. \tag{20}$$

Equation (20) follows from (16)*. Figure 5 shows the result obtained for two different crystal samples K 1 and K 2. The experimental data were normalized with respect to the power of the unfocused laser beam cross section at the $1/e^2$-positions. The beam power of the focused laser was determined by a procedure proposed by Schwiesow [14]. This normalization procedure turned out to be rather precise and it could be used also in order to determine the γ-function for polariton scattering experiments. The power density within the active scattering volume in such experiments cannot be calculated

* We have used the fact that I_∞ generally turned out to be $\approx I_0/2$, see below.

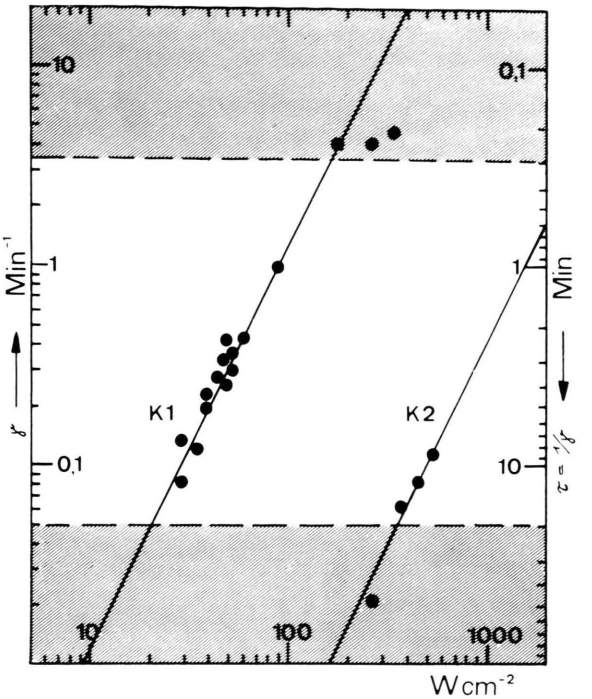

Fig. 5. Dependence of the time constant γ and $\tau \equiv 1/\gamma$ on the laser power density within the active Raman scattering volume, see Eqs. (16) and (20). Experimental data for two different samples K 1 and K 2 with different Fe-impurity concentrations are shown.

by simple geometrical considerations any longer because the *recorded* polariton intensities no longer are caused by a radial symmetric Gaussian beam. In the upper hatched area of Fig. 5 the experimental determination of the time constant became uncertain because $\tau = 1/\gamma \leqq 20$ sec. In the lower hatched area with $\tau = 1/\gamma > 20$ min, on the other hand, the recorded phonon intensities did hardly change any more because the shape of the scattering volume remained almost constant. In order to prevent confusion with the more detailed discussion of $I(t)$ below, we point out that γ plotted in Fig. 5 always was determined from the very first intensity drop $\mathrm{d}I/\mathrm{d}t$ which still could be represented by an exponential function.

Figure 5 shows that γ as a function of laser output power is different for the two samples. Light scattering experiments therefore seem to provide a method allowing the determination of Fe-impurity concentrations in $LiNbO_3$. Our present experiments, however, do not yet allow a quantitative analysis because the number of samples studied by us still was too limited.

The experiments described so far allow an estimation of the refractive index change on the basis of geometrical data. We typically measured $y = R_\infty/R_0 = 3/2$, and $x = 23$. Equation (11) then provides $\Delta n_\infty = 0.008$, an order of magnitude which agrees well with other data from the literature.

b) Phonon Scattering Intensities

Phonon intensities were recorded by the conventional right angle scattering technique. Figure 6 shows the time dependence $I(t)$ of the A_1(TO)-phonon at 632 cm^{-1} for varying laser power in the focus. In agreement with the observed deformation of the laser path the scattering intensity decreases from I_0 and reaches I_∞ after a few minutes. I_∞ was found to be $\approx I_0/2$. Our entrance slit was $S = 4\ cm^{-1}$ and the laser was focused into the sample by an $f = 8$ cm-lens. The ratio I_0/I_∞ of course depends on the specific scattering geometry. It could be verified, however, that I_0/I_∞ was independent from the laser output power within an error of $\pm 15\%$. Since the photon induced change of the extraordinary refractive index remained also after the illumination all curves in Fig. 6 were recorded by using different light paths through the sample. In contrast to the graphs shown in Fig. 4 the curves recorded with higher power in the laser focus all pass a minimum before I_∞ is reached. This effect can be described as the aperiodic limit of a damped oscillation. A indication of corresponding damped oscillations has been observed previously by means of a direct holographic technique [4].

We succeeded in recording damped cut-in oscillations by illuminating the sample alternating with extraordinary and ordinary photons, Figure 7. The graphs in this figure demonstrate that the extraordinary refractive index change can be reset in part by illuminating the damaged scattering volume with ordinary photons. Ordinary laser light obviously influences the optically damaged regions of the sample. It does not influence the undamaged regions remarkably.

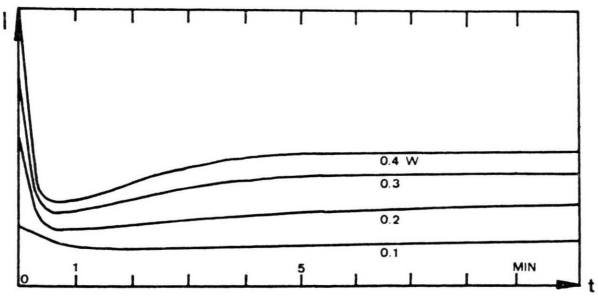

Fig. 6. Time dependence of the scattering intensity of the A_1(TO)-phonon in $LiNbO_3$ for different laser power. The detailed shape of the curves depends on the scattering geometry used for registration. The laser was focused into the sample by an $f = 8$ cm lens. Entrance slit width $= 4\ cm^{-1}$.

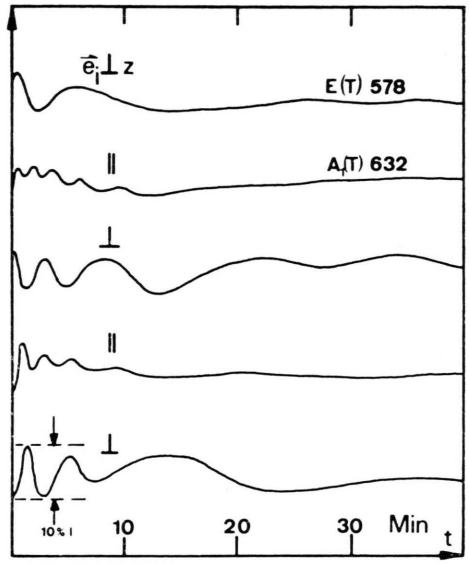

Fig. 7. Cut-in oscillations of the Raman scattering intensity caused by initial fluctuations of Δn at higher laser intensities in the focal region. The scans demonstrate that the extraordinary refractive index change can be partly reset by illuminating the sample with ordinary laser polarization, see text. The scattering geometries used when recording the E(TO)- and A_1(TO)-phonons, respectively, were $y(xz)x$ and $y(zz)x$. Kr^+-laser output power $P_L = 500$ mW.

After the stationary scattering intensity I_∞ of the 632 A_1(TO)-phonon had been reached the laser polarization was changed from $\boldsymbol{e}_i \parallel z$ to $\boldsymbol{e}_i \perp z$. The light path through the sample was left unchanged. The uppermost curve in Fig. 7 shows the oscillating time dependence of Raman scattering from the ordinary E(TO)-phonon at 578 cm^{-1} then recorded. After a few oscillations its constant value I_∞ was achieved. When changing back the polarization to $\boldsymbol{e}_i \parallel z$ cut-in oscillations of the A_1(TO)-phonon appeared again. The changed extraordinary refractive index thus had been influenced by ordinary photons. The phenomenon was reproducible when altering the laser polarization from $\boldsymbol{e}_i \parallel z$ to $\boldsymbol{e}_i \perp z$ and vice versa several times as shown in Figure 7. ΔI turned out to be of the order $\pm 5\%$. Equivalent results were obtained also when recording Raman scattering from other phonons of A_1- and E-type. The intensity oscillations are caused by the optical

refractive index change only. They obviously had no lattice dynamical origin. We therefore conclude that the oscillating intensities indicate that the excited electron could also approaches its final shape within and around the laser beam path by a damped oscillation. The observed phenomenon seems to provide a method to obtain information on the mobility of excited electrons from impurities in $LiNbO_3$ and other corresponding insulators.

The phonon scattering intensity as a function of the position of the scattering centre within the optically damaged path through the sample finally has been studied too. $I(x)$ gives important supplementary information confirming our geometrical microscopic interpretation of the origin of $I(t)$. The laser was focused by a $f = 30$ cm lens into the sample. After the stationary value I_∞ had been reached (~ 20 minutes) the sample was moved perpendicularly to the beam direction y by steps of 0.125 mm in the $-x$ or $+x$ direction. Raman scattering was recorded for a few seconds only in order to avoid a remarkable change of the optically damaged scattering volume. Figure 8 shows the intensity function $I = I(x)$ obtained in this way. A significant variation of $I(x)$ takes place within a narrow region of $\Delta x \approx 1$ mm only. This agrees well with the shape and dimensions of the scattering volume after long time illumination. Study of the sample with a microscope allowed a direct visual observation of the optically damaged region and its dimensions too.

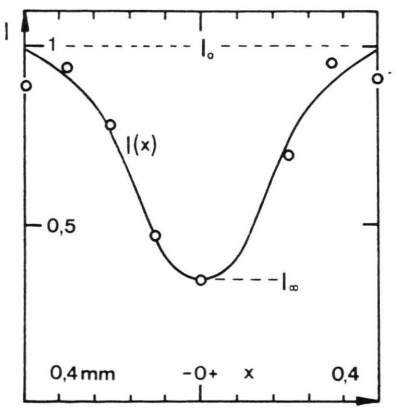

Fig. 8. Spatial distribution of extraordinary phonon scattering intensities $I(x)$ within the optically damaged scattering volume. Laser beam direction = y. The coordinate x measures a direction perpendicular to y and the extraordinary laser polarization z. The graph shows the intensity of the A_1(TO)-phonon at 253 cm^{-1}.

c) Polariton Scattering Intensities

We finally turn our attention to the time dependence of polariton scattering intensities caused by the photorefractive effect. Light scattering from polaritons is usually recorded by very near forward scattering geometries when exciting lasers in the visible are used. Momentum conservation causes the observation of elementary excitations with wave vectors of the order of only $10^3 \lesssim k \lesssim 2 \cdot 10^4$ cm^{-1}, see e.g. [15]. When regarding Figs. 2 and 3 it is realized immediately that the changing shape of the laser beam path must influence polariton scattering intensities severely. Phonon intensities as a function of time always ended up at a constant limiting value I_∞ not withstanding the cut-in behaviour was purely exponential, a damped oscillation or its aperiodic limit. Polariton intensities $I(t)$, however, generally showed a periodic undamped break down which was observed over many hours. Figure 9 shows the phenomenon for varying laser output power. The "oscillation" time T as well as the amplitude I increased with decreasing laser power. It was found to be up to 40% of the minimum value I_∞ defined in Figure 9a. Although the quantitative results again were sample dependent,

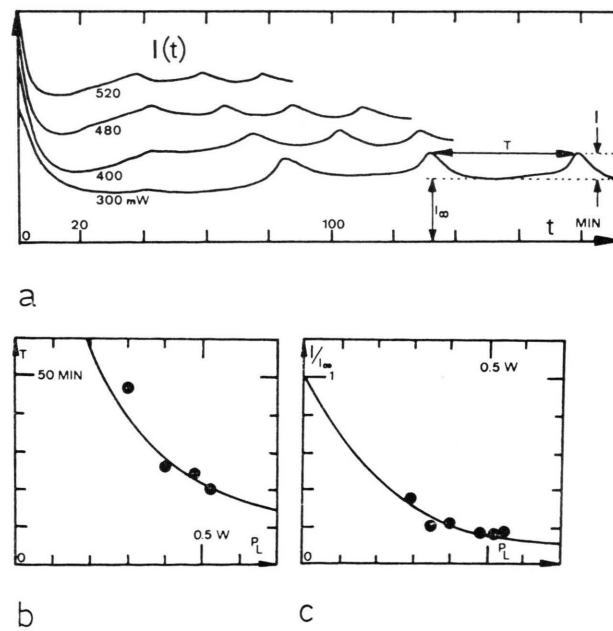

Fig. 9. a) Time dependence of polariton scattering intensities ending up in an undamped "oscillation", see text. b) and c) Observed oscillation time T, and intensity ratio I_0/I_∞ as a function of the laser output power, respectively.

the effect in principle was observed in all crystals studied by us. The scans in Fig. 9a correspond to a polariton mode at 155 cm^{-1} which is associated with the A_1(TO)-phonon at 253 cm^{-1}. Figure 9b and 9c show the recorded "oscillation" time T and the intensity ratio I/I_∞ as a function of P_L quantitatively.

It is well known that simultaneously with polariton scattering in near forward directions, always some phonon scattering in backward direction is recorded. This happens because the laser beam is partly reflected on the second surface inside the sample and because back scattered light becomes reflected on the first inner surface so that it also can reach the entrance slit [15]. The recorded time dependence of the "back scattered" phonon intensity showed the inverse behaviour: When the polariton intensity had a maximum, the back scattered phonon intensity showed a minimum. This behaviour was observed both for extraordinary and ordinary polaritons and their backscattered phonons. Figure 10 gives a survey. Note that the *ordinary* lattice modes reproduced there were recorded by the geometry $y(zx)y$. The incident laser thus was polarized parallel to the optic axis (= *extraordinary* photons!). To the left in Fig. 10 an A_1(TO)- and an E(TO)-spectrum recorded by near forward scattering are shown. The (almost) coinciding intensity maxima and minima of polaritons and back scattered phonons are shown to the right. The polariton intensity maxima have been hatched there in order to allow better orientation. The scans intend to demonstrate the coincidences in time only. Relative intensities may not be compared because every mode was always recorded with maximum sensitivity. The identity of the peaks is given with the spectra to the left. The origin $t = 0$ has been fixed and indicated by one maximum of the polariton mode at 155 cm^{-1} only. The pulse sequences turned out to be surprisingly constant: $T \pm 20\%$. All the features described could be observed unambiguously only for $\boldsymbol{e}_i \parallel z$-polarization of the exciting laser beam, which is in agreement again with b) in the introduction.

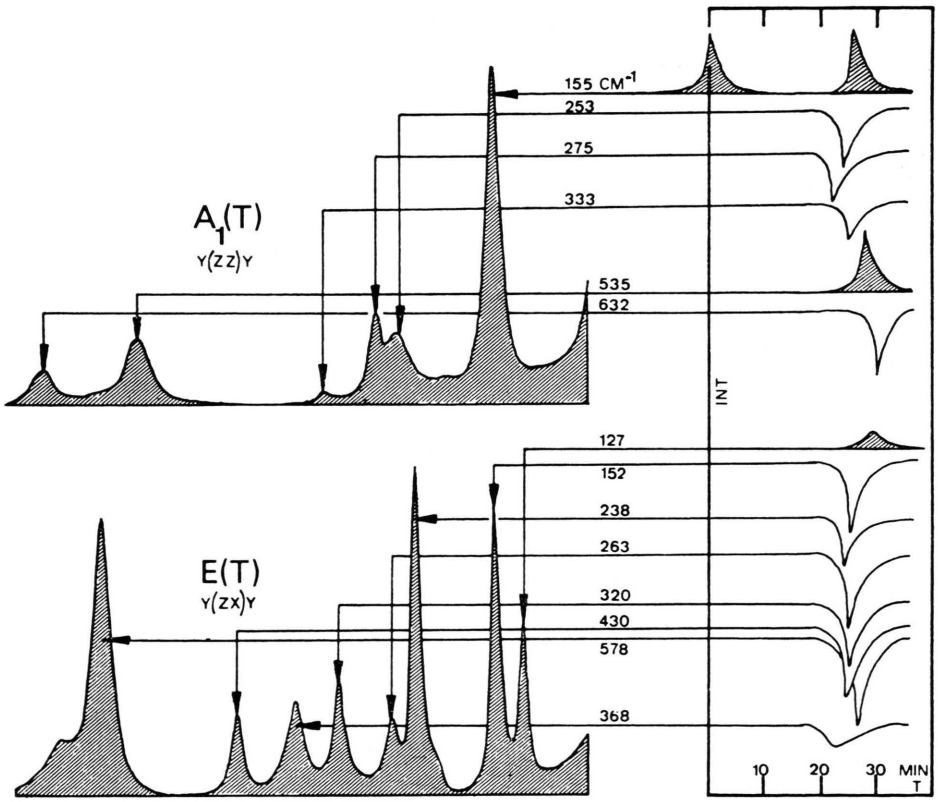

Fig. 10. Inverse intensity oscillations of polaritons and back scattering by phonons. The hatched peaks to the right in the figure indicate polariton intensity maxima. The spectra to the left allow the identification of the peaks.

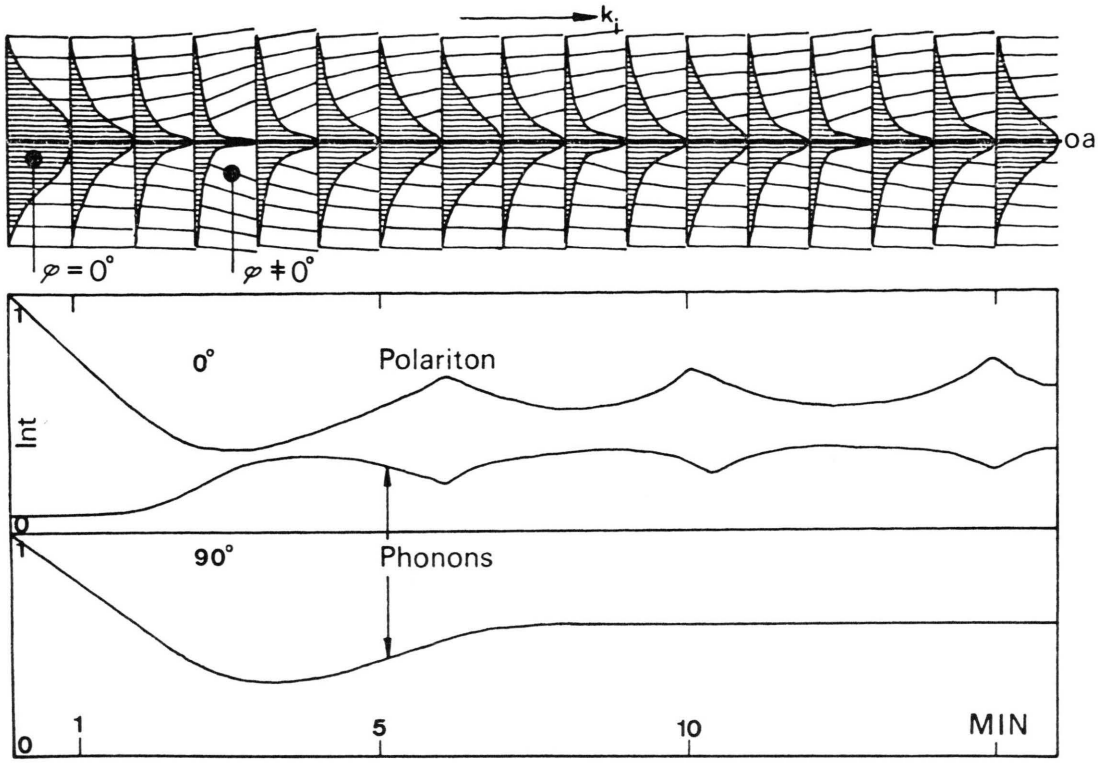

Fig. 11. Interrelation between the recorded intensity oscillations of polaritons or "back scattered phonons" and the direction of incident photons within the scattering volume, see text for a detailed discussion.

The undamped "oscillations" observed by near forward scattering can be explained by means of Fig. 11 as follows:

In the lower part of Fig. 11 three scans have been reproduced showing representative oscillating intensity functions of polaritons, "back scattered" phonons, and phonons recorded by right angle scattering. The hatched Gaussian curves above indicate the part of the cross section of the laser beam inside the sample with photons propagating parallel to the optic axis (oa) of the system (not crystal!). These photons give rise to time dependent polariton scattering at the Raman frequency recorded. Initially the laser intensity in the centre of the scattering volume is very high. The probability for excited electrons to be captured by Fe^{3+}-ions in the focus is small. They all remain in the conduction band and move away from the laser focus with a finite velocity. Consequently a very high local electric field is built up causing a strong change of the refractive index. This in turn causes the laser beam to diverge to a cylinder, Figure 3. The number of photons propagating parallel to the axis oa ($\varphi = 0$) decreases and of those propagating with a weak divergence ($\varphi \neq 0$) relative to oa increases.

The intensity of the polariton mode is expected to decrease. The scattering intensities of the "back scattered" phonons should increase, however, because they originate essentially from slightly divergent laser light integrated over a certain space angle in backward direction after the reflection. This is easily verified by checking the scattering geometry, see e.g. [15]. The frequency of phonon modes at large wave vectors ($k \approx 10^5\ \mathrm{cm}^{-1}$) is almost independent of k so that a spatial integration over a large k-region (experimentally = space angle) amplifies the intensity at only one specific frequency: that of the phonon mode!

The high electric field built up by the electron motion finally gives rise to an electric break down causing a part of the electron cloud to jump back to the initial beam centre. The index change is partly reset and the laser cylinder converges until the procedure repeats. These undamped break downs have not been reported hitherto. The

phenomenon is not expected to be observable by right angle scattering because the optically induced variation of the phonon wave vector k then is small compared with k itself.

All experiments have been carried out by a Kr^+-laser ($\lambda = 647.1$ nm). None of the described phenomena could be recorded when exciting the spectra by Nd:YAG-laser radiation in the infrared ($\lambda = 1.06$ μm) which is in agreement with the results reported in [6].

Acknowledgement

We thank Dr. E. Wiedendanger, ETH Zürich, for providing us with $LiNbO_3$-samples and the Deutsche Forschungsgemeinschaft for the Kr^+-laser.

[1] D. Redfield and W. J. Burke, J. Appl. Phys. **45**, 4566 (1974).
[2] M. G. Clark, F. J. Di Salvo, A. M. Glass, and G. E. Peterson, J. Chem. Phys. **59**, 6209 (1973).
[3] D. L. Staebler and W. Phillips, Appl. Opt. **13**, 788 (1974).
[4] G. E. Peterson, A. M. Glass, and T. J. Negran, Appl. Phys. Lett. **19**, 130 (1971).
[5] H. B. Serreze and R. B. Goldner, Appl. Phys. Lett. **22**, 626 (1973).
[6] F. S. Chen, J. Appl. Phys. **40**, 3389 (1969).
[7] R. L. Townsend and J. T. La Macchia, J. Appl. Phys. **41**, 5188 (1970).
[8] P. A. Arsenev and B. A. Baranov, Phys. Stat. Sol. **9a**, 673 (1972).
[9] M. Born and E. Wolf, Principles of Optics, Pergamon Press, New York 1959, p. 111.
[10] L. Montagnino, J. Opt. Soc. Amer. **58**, 1667 (1968).
[11] F. R. Mc Carnon, R. H. Muller, and C. W. Tobias, J. Opt. Soc. Amer. **65**, 1011 (1975).
[12] K. W. Beach, R. H. Muller, and C. W. Tobias, J. Opt. Soc. Amer. **63**, 559 (1973).
[13] F. P. Kapron, J. Opt. Soc. Amer. **60**, 1433 (1970).
[14] R. L. Schwiesow, J. Opt. Soc. Amer. **59**, 1285 (1969).
[15] R. Claus, L. Merten, and J. Brandmüller, Light Scattering by Phonon-Polaritons, Springer Tracts in Modern Physics, Vol. **75**, 1975.
[16] H. Kurz, E. Krätzig, W. Keune, H. Engelmann, U. Gonser, B. Dischler, and A. Räuber, Appl. Phys. **12**, 355 (1977).